Atmos. Chem. Phys. Discuss., 11, 33191–33227, 2011
www.atmos-chem-phys-discuss.net/11/33191/2011/
doi:10.5194/acpd-11-33191-2011

Atmospheric Chemistry and Physics Discussions

Total depletion of ozone reached in the 2010–2011 Arctic winter as observed by MIPAS/ENVISAT using a 2-D tomographic approach

E. Arnone[1], **E. Castelli**[1], **E. Papandrea**[2], **M. Carlotti**[2], **and B. M. Dinelli**[1]

[1]Istituto di Scienza dell'Atmosfera e del Clima – CNR, Bologna, Italy
[2]Dipartimento di Chimica Fisica e Inorganica, Università di Bologna, Italy

Received: 26 July 2011 – Accepted: 17 November 2011 – Published: 16 December 2011

Correspondence to: E. Arnone (e.arnone@isac.cnr.it)

Published by Copernicus Publications on behalf of the European Geosciences Union.

Abstract

We present observations of the 2010–2011 Arctic winter stratosphere from the Michelson Interferometer for Passive Atmospheric Sounding (MIPAS) onboard ENVISAT. Limb sounding infrared measurements were taken by MIPAS during the Northern polar winter and into the subsequent spring, giving a continuous vertically resolved view of the Arctic dynamics, chemistry and polar stratospheric clouds (PSCs). We adopted a 2-D tomographic retrieval approach to account for the strong horizontal inhomogeneity of the atmosphere present under vortex conditions, self-consistently comparing 2011 to the 2-D analysis of 2003–2010. Unlike most Arctic winters, 2011 was characterized by a strong stratospheric vortex lasting until early April. Lower stratospheric temperatures persistently remained below the threshold for PSC formation, extending the PSC season up to mid-March, resulting in significant chlorine activation leading to ozone destruction. Through inspection of MIPAS spectra, 84 % of PSCs were identified as supercooled ternary solution (STS) or STS mixed with nitric acid trihydrate (NAT), 16 % formed mostly by NAT particles, and only a few by ice. In the lower stratosphere at potential temperature 450 K, vortex average ozone showed a daily depletion rate reaching 100 ppbv day^{-1}. In early April at 18 km altitude, 10 % of vortex measurements displayed total depletion of ozone, and vortex average values dropped to 0.6 ppmv. This corresponds to a chemical loss from early winter greater than 80 %. Ozone loss was accompanied by activation of ClO, associated depletion of its reservoir $ClONO_2$, and significant denitrification, which further delayed the recovery of ozone in spring. Sporadic increases of NO_2 associated with evaporation of sedimenting PSCs were also observed. Once the PSC season halted, ClO was reconverted into $ClONO_2$. Compared to MIPAS observed 2003–2010 Arctic average values, the 2010–2011 vortex in late winter had 15 K lower temperatures, 40 % lower HNO_3 and 50 % lower ozone, reaching the largest ozone depletion ever observed in the Arctic. The overall picture of this Arctic winter was remarkably closer to conditions typically found in the Antarctic vortex than ever observed before.

ACPD

11, 33191–33227, 2011

1 Introduction

In the early 1980s, the discovery of a major ozone loss in the Antarctic spring (Farman et al., 1985), the so called ozone hole, led to an unprecedented international effort to understand and regulate the impact of ozone depleting substances on the protective ozone layer (WMO, 2007). The key mechanisms of ozone depletion were soon related to chlorine compounds and polar stratospheric clouds (PSCs) in the very cold and undisturbed Southern polar vortex (Solomon et al., 1986). The formation of nitric acid trihydrate (NAT), supercooled ternary solution (STS), and ice PSCs provides both the surfaces needed for heterogeneous chemistry and a means for removal of HNO_3 and H_2O through temporary capture and sedimentation (Solomon, 1999). Heterogeneous chemistry on PSC particles converts chlorine reservoirs $ClONO_2$ and HCl into Cl_2. In the sunlit Antarctic spring, chlorine is converted into active radicals such as Cl and ClO, which destroy most of the vortex ozone at 14–20 km altitude (Solomon et al., 1986; Molina et al., 1987). The destruction occurs at a much faster rate than the slow gas-phase nitrogen cycles driving depletion in the layers above. Additional reactions with BrO compounds contribute to ozone depletion in the lowermost stratosphere. Denitrification of the Antarctic stratosphere through sedimentation of HNO_3 prevents the reactive NO_x to promptly recapture the available chlorine into reservoirs, which in turn would halt the depletion (see the review by Solomon, 1999). Radiative feedback of the Antarctic ozone hole was also proposed to further extend the persistence of low temperatures, significantly delaying the spring ozone recovery (Randel and Wu, 1999).

The same basic ozone depleting mechanisms are at play also in the Arctic (Solomon, 1999; WMO, 2007). The total ozone depletion in the Arctic winter was found to be linearly dependent on the volume of PSCs integrated over the winter (Rex et al., 2006), a relationship that was recently proved to apply also to individual stratospheric layers (Harris et al., 2010). Large planetary wave disturbances (Andrews et al., 1987) usually prevent very cold temperatures to persist in the Northern polar vortex, so that PSC

ACPD
11, 33191–33227, 2011

occurrence in the Arctic is limited to smaller air volumes and shorter periods. As a consequence, ozone depletion in past Arctic winters did not reach the magnitude observed over the Antarctic. The observed Arctic total ozone loss in past years ranged between 25–35 % in very cold winters (such as in 1995–1996, 1999–2000 and 2004–2005) to almost none in warmer winters (WMO, 2007; Kuttippurath et al., 2010). In particular, 1995–1996 showed the coldest Arctic temperatures of the previous 17 yr extending until early March, with associated ozone loss of about 2/3 of that observed in Antarctic over an equivalent period (Manney et al., 1996). In 1999–2000 Arctic winter, ozone loss reached 70 % in a narrow layer of the lower stratosphere (Rex et al., 2002). In 2004–2005, ozone was affected by the largest loss reported for past winters, halted by a stratospheric warming in early March so that the magnitude of Antarctic ozone loss was not matched (e.g. Manney et al., 2006). Eventually, Arctic ozone hole conditions were reported for the 2010–2011 Arctic winter (Manney et al., 2011).

In this paper, we present observations of the 2010–2011 Arctic winter taken by the Michelson Interferometer for Passive Atmospheric Sounding (MIPAS) onboard the polar orbiting ENVISAT satellite (Fischer et al., 2008). MIPAS has proven to be a suitable instrument for detailed studies of polar stratospheric processes including observation of PSCs and their composition (Höpfner et al., 2006). MIPAS observations were analysed with a 2-D tomographic retrieval (the Geofit-Multi Target Retrieval (GMTR) by Carlotti et al., 2006) to correctly account for along-track horizontal inhomogeneities. The resulting data (MIPAS2D, Dinelli et al., 2010) were proven to greatly reduce the spurious anomalies induced by horizontal gradients adopting 1-D codes (Kiefer et al., 2010), and are therefore more suitable under vortex conditions. The structure of the paper is as follows: Sect. 2 presents the MIPAS experiment, the MIPAS2D data, the PSC detection method, and the adopted meteorological products. MIPAS observations of the vortex dynamics, PSCs and chemical evolution of the Arctic stratosphere are presented in Sect. 3. The results are discussed in Sect. 4 in comparison to previous Arctic winters and typical Antarctic conditions. Conclusions are given in Sect. 5.

ACPD
11, 33191–33227, 2011

2 Data and methodology

2.1 MIPAS

MIPAS is part of the payload of Europe's Environmental monitoring satellite, ENVISAT, launched on 1 March 2002. ENVISAT was injected into a polar orbit at an angle of 81.5° and altitude of about 800 km. The orbital period is about 101 min achieving a global coverage of the Earth with 14.3 daily sun-synchronous orbits with the descending (North to South) part crossing the Equator at approximately 10:00 local time (LT) and the ascending part crossing it at approximately 22:00 LT (hereafter labelled am and pm measurements). MIPAS is a limb-scanning Fourier Transform (FT) spectrometer recording the emission of the atmosphere in the mid-infrared, with a spectral range extending from 680 to 2410 cm^{-1} (14.6–4.15 µm) and an instantaneous field of view of approximately 3 km in height and 30 km across track at tangent point. Most of its measurements are taken with an along track backward looking configuration, with a sideward deviation at high latitudes allowing MIPAS to measure up to 89.3° N and 87.5° S. During the original full resolution (FR) mission, MIPAS was operated with a spectral resolution of 0.035 cm^{-1} full width half maximum, unapodised. The FR mission covers the time period from July 2002 to March 2004, when MIPAS operations in the original configuration were suspended due to the deterioration of the interferometric slides. Starting from January 2005, MIPAS operations have been resumed in the optimised resolution (OR) mission, with the instrument operating at 41 % of its maximum spectral resolution. The complete nominal limb scanning sequence (scan) of the original FR mission consists of 17 spectra with nominal tangent points ranging from 6 to 68 km, and a horizontal separation between adjacent scans of about 500 km (~4.6 degrees in latitude). In the OR nominal observation mode, each scan is made of 27 limb views with tangent altitudes ranging from 6 to 70 km at variable altitude steps. The OR scan pattern corresponds to a horizontal separation between adjacent scans of about 410 km (~3.7 degrees in latitude). A more detailed description of the MIPAS experiment can be found in Fischer et al. (2008).

ACPD
11, 33191–33227, 2011

2.2 MIPAS2D data

We retrieved MIPAS level 2 products with the Geo-fit Multi-Target Retrieval (GMTR) tomographic analysis tool (Carlotti et al., 2006). GMTR is based on the Geo-fit approach (Carlotti et al., 2001) upgraded with the Multi-Target Retrieval (MTR) functionality (Dinelli et al., 2004). The Geo-fit approach enables to take into account the horizontal atmospheric inhomogeneities performing a tomographic retrieval on observations collected along a whole orbit through a 2-D discretization of the atmosphere. The 2-D approach assumes the atmosphere homogeneous only across the orbit track, with the maximum extent corresponding to the distance of MIPAS tangent points from their along track projection (up to 2° latitude). The capability of the GMTR system to model the horizontal structures of the atmosphere makes its application to MIPAS measurements particularly suitable for the work presented in this paper that is focused on the polar winter regions, where strong horizontal gradients are present. The MTR approach, by simultaneously fitting pressure, temperature and some interfering species, allows a reduction of the systematic error components due to the propagation of the uncertainties on pressure, temperature and on the amount of molecules that generate interfering spectral features. An upgraded version of the GMTR system was applied by Dinelli et al. (2010) to MIPAS observations to generate the MIPAS2D database. MIPAS2D can be found at http://www.mbf.fci.unibo.it/mipas2d.html and mirrored at http://www.isac.cnr.it/~rss/mipas2d.htm (hereafter MIPAS2D website). The MIPAS2D database consists of 2-D fields of pressure (p), temperature (T), and volume mixing ratio (VMR) of the six high priority species H_2O, O_3, HNO_3, CH_4, N_2O, and NO_2, covering MIPAS complete mission. The database, thoroughly described in Dinelli et al. (2010) and Papandrea et al. (2010), has been used as a starting point for this analysis. The 2-D fields were obtained on a fixed vertical grid (spanning the altitude range from 6 to 42 km in steps of 3 km, and upward at altitudes of 47, 52, 60 and 68 km), and on a horizontal equispaced grid of 5° in latitude. Because of their correlations, p, T and H_2O were jointly retrieved with O_3, followed by the sequential retrieval of the VMRs of

ACPD
11, 33191–33227, 2011

the other molecules listed above. The quality of MIPAS2D data for these key species was described in Dinelli et al. (2010).

For this work, we have upgraded the MIPAS2D database by analysing the newly delivered MIPAS level 1b data where both FR and OR missions were processed with the same Instrument Processing Facility version 5.05. This version was shown to improve the previous processing, and, most importantly, to lead to a correct altitude determination validated by comparison to radiosonde data (see e.g. Tomasi et al., 2011). Biases may be caused by the different retrieval configuration needed for the different spectral resolution of the FR and OR MIPAS measurements. To avoid this, the FR spectral resolution was numerically degraded to the resolution of the OR mission, so that the same set of spectral intervals (microwindows) could be used throughout the whole MIPAS mission. Reference average error profiles for the new processing of these key species are reported on the MIPAS2D website. Additionally, we have also individually retrieved $ClONO_2$ and ClO in cascade following the main targets. The spectral microwindows used for this new analysis are listed on the MIPAS2D website. For the additional species the random error is on the order of 5–10 % for $ClONO_2$ and 50 % for ClO, depending on altitude, latitude and period of the year. The large error on ClO is due to its very weak spectral signal (often below the noise level). Averages of ClO data have been performed including only am measurements, with daylight conditions depending on the location of the measurement as compared to the day-night terminator. The influence of the adopted a-priori profile on the retrieved ClO cannot be neglected, therefore care should be taken when dealing with absolute values. For all MIPAS2D quantities used in this work, data were filtered on the basis on the information gain parameter discussed in Dinelli et al. (2010) and excluding cloud-contaminated spectra. When MIPAS lines of sight crossed thick PSCs (see next section), information was derived from nearby clean measurements by the tomographic retrieval. Regions of very dense PSC coverage prevented a detailed chemical analysis. For most of the analysis, MIPAS2D data were linearly interpolated onto potential temperature levels calculated from coincident MIPAS2D pressure and temperature.

ACPD
11, 33191–33227, 2011

2.3 PSC detection and composition

As discussed, cloud-contaminated spectra are excluded from the GMTR analysis since they can deteriorate the quality of the retrieved parameters. However, the sensitivity of MIPAS to the radiation emitted and scattered by the clouds can be exploited to study PSCs, since MIPAS limb views are sensitive to very optically thin clouds, both during day and nighttime. PSCs can be detected exploiting the cloud index (CI) technique (Remedios and Spang, 2002). The CI is the ratio of the average spectral radiances in the 788–796 cm^{-1} range (where gas absorption is dominant) and in the 832–834 cm^{-1} range (where clouds effects dominate). The ratio is sensitive to the presence of any type of cloud, with lower values associated to increasingly optically thicker clouds. To detect PSCs into MIPAS spectra, we used a CI threshold of 4.5 (Spang et al., 2005) combined with a lower altitude threshold of 16 km to avoid the inclusion of high altitude tropospheric clouds, and an upper altitude limit of 35 km to minimise false detections. The CI threshold corresponds to a lower detection limit of PSCs with volume density of about 0.2 $\mu m^3\,cm^{-3}$ (Höpfner et al., 2006). The tangent altitude of the highest cloudy spectrum in a limb scan was used as an approximated cloud top height (CTH). The error on the determined CTH can be assumed as ±1.5 km, i.e. about half of the vertical sampling step of MIPAS OR scans or of the vertical projection of the field of view at tangent point (3 km). The CI method has been validated by Höpfner et al. (2009) using the Cloud-Aerosol Lidar and Infrared Pathfinder Satellite Observation (CALIPSO), with MIPAS identifying about 70 % of the PSCs detected by CALIPSO in the Arctic winter.

To determine the PSC composition we applied the methodology developed for MIPAS by Höpfner et al. (2006). The method is based on the NAT spectral signature at 820 cm^{-1} and on the effects due to the large optical depth of ice particles. A new CI (called from now on NAT index) was defined as the ratio between the average intensity over the 819–821 cm^{-1} spectral range and the average intensity over the 788–796 cm^{-1} range. Following Höpfner et al. (2006, 2009), PSCs can be classified in three groups based on their composition: ice, NAT and STS/Mix. The classification is

ACPD
11, 33191–33227, 2011

performed through a diagram of the color ratio of the NAT index versus the CI index (see Höpfner et al., 2006, Fig. 9). The PSCs classified as ice include mainly PSCs formed by ice particles only. The PSCs classified as NAT are made of at least 30–40 % of NAT particles with mean radius smaller than 3 µm. The PSCs classified as STS/Mix include PSCs which are most likely STS, but can also be of mixed compositions having a minor contributions from NAT or ice. Also PSCs made of very thin ice particles or large NAT particles were shown to fall within the last category because of their spectral signature similar to the pure STS case. The STS/Mix should therefore be considered as a mixture of STS, NAT and ice PSCs. Comparison of the PSC composition derived from MIPAS, CALIPSO and lidar by Höpfner et al. (2009) confirmed that the PSCs classified as MIPAS NAT are made of non spherical solid particles, the MIPAS ice are largely made of ice, and MIPAS STS/Mix are a mixture of liquid STS and NAT particles.

2.4 ECMWF meteorological products

In this paper, the vortex edge was identified by using the scaled potential vorticity (sPV, s^{-1}, Manney et al., 1994) derived from the European Centre for Medium-Range Weather Forecasts (ECMWF) meteorological products. Vortex average quantities were made on the basis of sPV greater than $1.7 \times 10^{-4}\,s^{-1}$. The adopted value is slightly higher than that adopted e.g. by Manney et al. (2006) and allowed a more conservative selection of low in-vortex N_2O values at all potential temperature levels in the stratosphere as compared to lower sPV values. In equipotential maps, the outer and inner vortex edges were shown adopting $sPV = 1.4 \times 10^{-4}\,s^{-1}$ and $2 \times 10^{-4}\,s^{-1}$. ECMWF sPV values were extracted from the 12 universal time (UT) fields, and could therefore lead to a mismatch between MIPAS observations (performed at fixed local time due to the Sun-synchronous orbit) and the adopted vortex edge. However, a thorough inspection of MIPAS N_2O measurements at the vortex edge showed only minor deviations of the sPV and N_2O tracers, with negligible impact on the adopted vortex averages.

ACPD
11, 33191–33227, 2011

3 Observation of the 2010–2011 Arctic winter stratosphere

We studied the chemical and physical evolution of the Arctic stratosphere during the 2010–2011 winter analysing MIPAS measurements in the period from 1 December 2010 to 15 April 2011. The results of the analysis are presented here in terms of averages of the retrieved quantities inside the vortex and, for few significant cases, also as individual measurements. The results are discussed in Sect. 4.

To show the temporal evolution of the air masses inside the Arctic vortex, Figs. 1 and 2 report MIPAS2D data as vertical distribution of temperature, PSCs and VMRs of N_2O and O_3 (Fig. 1a to d), and of H_2O, HNO_3 and $ClONO_2$ (Fig. 2a to c). MIPAS2D data shown in the figure were obtained as daily averages within the vortex over isentropes with potential temperature (Θ) ranging between 350 and 1000 K (about 11 to 32 km altitude). Figure 1b reports the detected PSCs plotted over the average temperature of the region having $T < T_{NAT}$ (hereafter T_{NAT} region). The T_{NAT} temperature is the approximate threshold for PSC formation, and was calculated at each Θ level applying the empirical formula by Hanson and Mauersberger (1988) to MIPAS2D average H_2O and HNO_3. Figure 2d reports vortex average ClO at $\Theta = 550$ K from am measurements (blue line), at a level where errors were below 100 %. Figure 2d also reports the evolution of the vortex area in terms of fraction to its maximum extent of 25×10^6 km^2 (black dashed line) and the vortex sunlit daily fraction (red dashed line) both calculated at $\Theta = 550$ K.

The geographical behaviour of the vortex was studied by inspecting individual measurements of MIPAS over isentropic cross sections. As an example of the examined data, Fig. 3 reports snapshots at $\Theta = 500$ K of T, N_2O and O_3, for 3 and 26 February, 8 and 28 March 2011. Similarly, Fig. 4 reports snapshots of HNO_3 $ClONO_2$, and ClO. ClO is reported at 550 K consistently with Fig. 2d. In the two figures, the outer and inner vortex edges (black contour lines) are identified as described in Sect. 2.4. In January and February, the number of measurements contaminated by the presence of PSCs, that are rejected from the analysis, prevented a geographically detailed study at lower

ACPD
11, 33191–33227, 2011

Θ values. Only when PSCs disappeared in March the regions of deepest O_3 depletion around Θ = 450 K could be fully observed. The Θ = 500 K level was therefore chosen as a compromise between the Θ level showing the highest ozone depletion (around 450 K) and higher Θ levels having MIPAS spectra less affected by PSCs. We devote the next sections to the three main aspects characterising the 2010–2011 Arctic winter stratosphere, namely the vortex dynamics, PSC formation and chemical evolution.

3.1 Vortex dynamics

As shown in Fig. 1a and b, during the 2010–2011 winter a well defined and strong vortex led to regions of temperature below T_{NAT} lasting almost continuously until late March. The vertical extension of these vortex cold regions reached a very wide altitude range in early January, at Θ extending from 430 to 800 K, and then evolved to a progressively lower altitude range, down to Θ from 360 to 550 K in mid-March. Temperature minima dropped persistently below 185 K at Θ from 500 to 750 K in 2–7 January, and at Θ from 400 to 650 K in 20–28 January and sporadically throughout February. The presence of these persistent cold regions is reproduced in the vortex average temperature, displaying a minimum (cold point) below 195 K descending from about Θ = 600 K in early January to 450 K in mid-March (Fig. 1a).

Although the vortex was neither particularly centred nor symmetric (see the events shown in Fig. 3), following an expansion in early January (as shown by the black line in Fig. 2d), the vortex size remained relatively stable from mid January to April (around 20×10^6 km^2 at Θ from 450 to 550 K). The almost monotonical increase of the sunlit fraction of the vortex implies that the overall displacement of the vortex from the pole was very limited (red line in Fig. 2d). The isolation of the vortex air was well traced by the very low vortex values of N_2O (Fig. 1c) caused by the descent of upper atmospheric air. Vortex N_2O showed signs of mixing with outside vortex air only during a very few time-constrained warming events. The N_2O 100 ppbv isopleth, which will be used in the following sections to trace ozone chemical loss, descended from Θ = 550 down to 450 K from December to April (from about 21 to 18 km in altitude). The slow diabatic descent was consistently displayed also by H_2O (Fig. 2a).

ACPD
11, 33191–33227, 2011

Occasional planetary wave activity induced a deformation or displacement of the vortex (see Fig. 3), as reflected by the average vortex temperature and N_2O (Fig. 1a to c). For example on 3 February a sudden stratospheric warming (SSW) deformation, induced by a large planetary wave number-two, almost split the vortex into two lobes. This event was accompanied by warmer temperatures in the area where the two lobes were connected, with an indication of mixing with high N_2O values (visible as a peak of N_2O in Fig. 1c). Other relatively less intense events caused an elongation of the vortex followed by ejection of tongues of vortex air towards the outside regions, such as those occurring on 8 and 28 March and lasting a few days each (see Fig. 3). During the second event, the inner sPV contour line indicated ejection of air from inner regions of the vortex, resulting in about 10 % of vortex air between $\Theta = 400$ and 550 K being ejected. In the middle stratosphere, events leading to increased N_2O were only marginally reflected in the average temperature (see e.g. late January in Fig. 1a to c). This suggests these events were sporadic intrusions of outside vortex air with no major impact on the overall vortex isolation. A largely consistent behaviour was found using MIPAS2D CH_4 as passive tracer instead of N_2O, although further work is needed to understand a possible impact of chemistry on CH_4 in early spring. Towards early spring, two warmings accompanied the last phases of the vortex evolution, which was eventually displaced from the pole on 6 April and persisted as a large patch of isolated vortex air above Siberia and then Northern Europe until late April. Large concurrent increases in temperature and the N_2O tracer showed the Arctic return to typical conditions.

3.2 Polar stratospheric clouds

The vertical distribution of PSCs detected by MIPAS is reported in Fig. 1b. A total of 2920 MIPAS scans detected PSCs over the period 1 December 2010 to 18 March 2011, corresponding to 82 % of days with PSCs out of 92 days of observation. The 2010–2011 Arctic PSC season can be split into four main phases, each covering a relatively homogeneous vertical coverage: (i) 1–31 December 2010, with most PSCs occurring at $\Theta = 500$ to 600 K; (ii) 1–15 January 2011, showing an extraordinary vertical coverage up to $\Theta = 950$ K; (iii) 16 January–28 February, with the PSCs persistently ranging from

ACPD
11, 33191–33227, 2011

$\Theta = 400$ to 600 K; and (iv) 1–31 March 2011, characterised by more sporadic occurrence at $\Theta = 400$ to 500 K. Geographically, the bulk of PSCs clustered close to the cold core of the vortex for most of the winter, tracing the occasional distortion of its shape. The only evident deviation was observed between 20 and 29 January, when detected PSCs shifted from the cold core of the vortex to form a ring surrounding it.

The results of the analysis of the PSC composition for the four periods, based on Höpfner et al. (2006)'s method (see Sect. 2.3), are reported in Fig. 5a–d. In each color ratio diagram, gray lines delimit the three regions corresponding to PSCs classified as NAT, ice and STS/Mix (see labels in the figure). The color scale represents the difference ($T - T_{NAT}$) between the temperature coincident with the detected PSC and the estimated T_{NAT} threshold introduced above (red indicates $T > T_{NAT}$). Since MIPAS measurements contaminated by PSCs were rejected from the retrieval procedure, the temperature assigned to each PSC was taken from ECMWF. Temperatures 3 to 4 K below T_{NAT} can be considered as a threshold for STS formation (Stein et al., 1999). Figure 5 also reports snapshots of the geographical distribution of PSCs classified as NAT (red diamonds) or STS/Mix (white diamonds) for a selected day from each period (panels f to i). The snapshots also show the regions of expected formation of NAT (red line) and STS (white line) PSCs, calculated using ECMWF temperature (with the STS line at $T_{NAT} - 3.5$ K).

Beside some scattered PSCs detected in early December (see Fig. 1b), period (i) showed a very compact distribution of PSCs in the second half of the month. 90 % of PSCs were classified as STS/Mix, 10 % as NAT and none as ice (Fig. 5a). The temperature associated to each PSC was largely scattered, between 5 K below T_{NAT} to above it (see color scale in the figure), especially in the case of thinner clouds (high CI values). Although the majority of PSCs were vertically distributed where the average temperature was consistently around the threshold for STS formation (Fig. 1b), temperatures associated to the PSCs of this period were the highest of the 4 periods (compare Fig. 5a–d), pointing also to a possible NAT composition. During period (ii), the large vertical spread of the PSC distribution was reflected in their scattered spectral

ACPD
11, 33191–33227, 2011

characteristics (Fig. 5b). About 80 % of PSCs were classified as STS/Mix, 20 % as NAT and a very few cases as ice. The bulk of STS/Mix PSCs in the diagram was consistently associated with temperature below STS formation, and was observed between $\Theta = 450$ and 550 K (Fig. 1b). At Θ from 550 to 700 K, the STS/Mix PSCs had more scattered color ratio values and associated temperatures that reached values above T_{NAT}, therefore suggesting PSC formation within cold mesoscale temperature perturbations that were not reproduced by ECMWF temperatures (e.g. Carslaw et al., 1998). The large scatter in the color ratio implies very different mixtures in the PSC composition. The very high altitude clouds (CTH at $\Theta > 700$ K) detected during the very first days of January had either a clear STS signature (see bottom right of Fig. 5b) or extended towards the ice region (top left of the panel). In the clear STS cases, associated temperatures were largely above T_{NAT}, again supporting the importance of mesoscale perturbations that were likely missed by ECMWF temperatures. The few cases showing ice composition (top left of the panel, including also those around CI = 1.5), were found to be consistent with ECMWF temperature around the ice threshold, and represent the only ice PSCs detected during the whole season. In period (iii), the bulk of PSCs persisted at $\Theta = 500$–600 K and showed very compact spectral signatures in the diagram (Fig. 5c). 82 % PSCs were classified as STS/Mix, and 18 % as NAT. The highest PSCs were generally associated with very high CI values, implying very optically thin clouds. Consistent with the predominant STS composition, most PSCs falling in the STS/Mix portion of the diagram have an associated temperature 3 to 5 K below T_{NAT}. Comparison to vortex averaged temperature (Fig. 1a) shows PSCs occurred only where a large fraction of the vortex was colder than T_{NAT}. This suggests these PSCs were thick clouds associated with synoptic scales temperature (Adriani et al., 2004), a characteristic that is consistent with the stable and continue cold temperatures observed throughout February. During period (iv), PSCs were observed until 18 March and only around $\Theta = 400$–500 K (Fig.1b). Only 6 % of these late PSCs were classified as NAT, while 94 % as STS/Mix. The associated temperature also confirmed the STS/Mix composition.

ACPD
11, 33191–33227, 2011

A comparison of the location of the classified PSCs with NAT and STS regions predicted from ECMWF temperature showed an overall good agreement. Although not representative of the whole PSC population, Fig. 5e–h report some events with a remarkable consistency of the classified PSC and the expected NAT and STS regions also under very inhomogeneous conditions (see e.g. panels f and g), pointing to a general acceptable assignment of the PSC composition. As pointed out in Sect. 2.3, the NAT classification implies that the spectral signature of NAT particles was strong. This means that each of the PSCs we classified as NAT was composed of at least 40 % of such particles with mean radii smaller than 3 µm. On the contrary, the STS/Mix class indicates the presence of clouds which contain STS droplets, large NAT particles, or mixtures of the two. Since large NAT particles (3–6 µm) lead to very similar spectral signatures as STS, the STS/Mix class cannot rule out the possibility of having large NAT particles (or even NAT rocks, Fahey et al., 2001) in the corresponding cases. The presence of a fraction of observed clouds composed of STS droplets is suggested by the fact that coincident temperatures were largely below the STS formation threshold. The overall fraction of 16 % of NAT classified PSCs in the 2010–2011 Arctic winter can be therefore considered a good estimate of PSCs with dominant NAT composition.

3.3 Chemical evolution of the Arctic

In the following we present the chemical behaviour of the Arctic in terms of effects of changes of relevant trace gases and subsequent impact on O_3.

3.3.1 HNO_3 and H_2O

As a result of PSC formation, HNO_3 was significantly removed from the lower stratosphere from January to April (Fig. 2b). Vortex HNO_3 decreased from 10 to 4 ppbv within the isentropic range 450–500 K in which PSCs were continuously detected. In particular, the relatively higher vortex averaged HNO_3 following the SSW on 3 February, was promptly depleted by the successive persistent PSCs formation, with a 50 % drop in

ACPD
11, 33191–33227, 2011

about a month (Fig. 2b). During most of the winter, the lowest amounts of HNO_3 were found within or close to the cold core of the vortex, where the bulk of PSCs occurred (Fig. 4, top row). The low HNO_3 occurred where temperatures were below the STS formation threshold suggesting a capture by the NAT component of the STS/Mix PSCs (see Sect. 3.1). On some occasions, strips of NAT PSCs were clearly coincident with the deepest minima of HNO_3. Since the HNO_3 did not recover when the PSC season ended in mid-March, actual denitrification occurred in 2011. The observed low HNO_3 values can be therefore associated to both temporary sequestration by STS/Mix PSCs and to denitrification associated to PSCs composed of large NAT particles. Removal of HNO_3 at $\Theta = 450$–500 K was accompanied by sporadic increases of HNO_3 and NO_2 (not shown) at $\Theta = 400$–450 K, likely as a result of evaporation of sedimenting particles at lower level. As expected by the lack of ice PSCs, H_2O (Fig. 2a) showed only a marginal decrease in late March in the lower stratosphere. As mentioned in Sect. 3.1 the overall trend in H_2O was consistent with the diabatic descent. The lowest H_2O was reached in the second half of March at $\Theta = 400$–450 K, in coincidence with minima in HNO_3 and O_3, and increase in $ClONO_2$ (see below).

3.3.2 $ClONO_2$ and ClO

$ClONO_2$ was greatly depleted in the lower stratosphere at $\Theta = 400$–550 K (Fig. 2c) in January and February, then followed by a recovery in March. The largest depletion was coincident with the beginning of the marked decrease in HNO_3 starting in late December. The very low $ClONO_2$ in January was extended throughout the inner vortex, and accompanied by a collar of high values at the vortex edge (Fig. 4, middle row). The low $ClONO_2$ during February was accompanied by activation of ClO in the vortex, reaching a maximum in mid-March (Fig. 2d). This is also shown by ClO data at $\Theta = 550$ K (Fig. 4, bottom row), with ClO sporadic high values progressively increasing towards the more insolated outer regions of the vortex in February and more homogeneously distributed in March. Even then, ClO continued to be higher outside the centre of the vortex. Around 18 March, when the last PSCs disappeared, vortex-average ClO

ACPD
11, 33191–33227, 2011

started to dramatically decrease, accompanied by an analogous prompt increase in $ClONO_2$. At this late stage, $ClONO_2$ recovered throughout the vortex while patches of high ClO persisted in scattered regions of the vortex until early April.

3.3.3 O_3

Arctic vortex O_3 in 2011 was greatly depleted in the lower stratosphere at $\Theta = 400$–$500\,K$ (see Fig. 1d). At $\Theta = 450\,K$, vortex average O_3 dropped from 3 ppmv in early January to 0.95 ppmv in early April. Daily depletion rates reached 100 ppbv day^{-1} in mid-March. A second region of minimum was reached in the middle stratosphere at $\Theta = 700$–$800\,K$, with average O_3 decreasing from 4.5 ppmv in mid-January down to 3 ppmv in mid-March. The intermediate layer around $\Theta = 600\,K$ showed a very stable O_3. The meteorology of the 2011 Arctic vortex with the PSC season extending up to mid March played a key role in the lower stratosphere depletion (see Fig. 1b and d). Snapshots on the 500 K isentrope (about 20 km altitude) reported in Fig. 3 show depletion of O_3 occurring within the vortex since January with scattered low values on progressively larger areas of the vortex. O_3 depletion in February and March tended to be more pronounced in the outer parts of the vortex (see 28 March snapshot in Fig. 3), with occasional perturbations of the vortex causing a mixing with higher vortex values and leading to a more homogeneous distribution (see 8 March snapshot). The O_3 chemical loss was evaluated taking into account the descent of the N_2O 100 ppbv isopleth observed in Fig. 1c (Proffitt et al., 1990; Rex et al., 2002). Comparison of the minimum value of 0.95 ppmv reached by vortex averaged O_3 at $\Theta = 450\,K$ in early April to the 3.4 ppmv of O_3 at $\Theta = 550\,K$ in December following the evolution of the N_2O 100 ppbv isopleth (see Sect. 3.1) results in a chemistry-driven depletion of vortex O_3 of about 70 % at this level.

ACPD
11, 33191–33227, 2011

3.3.4 Measurement of total depletion of O_3 and HNO_3

The diagnostics adopted for this study involved interpolation on Θ levels. The interpolation may introduce a smoothing error in the vertical profiles, artificially removing sharp changes in the vertical gradient of the retrieved quantity. We therefore further investigated the occurrence of low O_3 and HNO_3 values in the original data retrieved on the fixed altitude grid (with relevant grid points at 15, 18 and 21 km – see Sect. 2). Figure 6a and c show timeseries of individual O_3 and HNO_3 VMR at the 18 km altitude grid point, both for vortex (blue) and outside vortex (gray) data North of 65° N. In March and early April, the 18 km altitude within the vortex corresponds to $\Theta = 460 \pm 12$ K, whereas $\Theta = 450$ K corresponds to an altitude of 17.8 ± 0.5 km. The difference in altitude falls therefore below the 3–4 km vertical resolution of the retrieved data. The O_3 timeseries show a progressively larger divergence between vortex and outside vortex values as the season evolved. While the distribution of vortex O_3 values at 18 km altitude was very compact until late March, in early April it displayed a much broader spread. This shows that O_3 started to recover in some parts of the vortex while it was reaching its deepest depletion in other parts. O_3 reached 100 % depletion in a fraction of the vortex in late March and early April. Figure 6 reports also the corresponding probability distribution functions (PDFs) calculated over 2 and 3 April. Vortex O_3 in early April had a relative flat distribution of VMR values extending from 0 to 1 ppmv. About 10 % of the vortex measurements at 18 km altitude are consistent with total depletion of O_3 within the measurement random error around 0.1 ppmv. The average vortex ozone at 18 km altitude dropped to 0.6 ppmv in 2–3 April. If compared to the average vortex O_3 in December at 21 km altitude grid point (i.e. along the 100 ppbv N_2O isopleth as discussed in the previous section), the drop corresponds to 80 % O_3 depletion.

Analogously, Fig. 6c shows the clear inhomogeneity in HNO_3. Loss of HNO_3 severely acted on a fraction of vortex air in late January and February, with greatly scattered low values, especially after the SSW on 3 February. It then turned into a more homogeneous low vortex HNO_3 in March and early April (Fig. 6d). The most severely depleted

ACPD
11, 33191–33227, 2011

individual measurements of vortex HNO_3 halted in early March in accordance with PSCs disappearing. Both for O_3 and HNO_3, error bars are shown for close to zero values to highlight their accuracy.

4 Discussion

In the following we discuss MIPAS2D observations of the 2010–2011 Arctic winter in comparison to previous Arctic winters and to typical Antarctic conditions.

4.1 Comparison to previous Arctic winters

The behaviour of the 2010–2011 Arctic winter stratosphere was compared to Arctic winters observed during MIPAS complete mission (from 2003 to 2010). Figure 7 reports timeseries of daily vortex averages of selected targets (see labels) at $\Theta = 450$ K for individual years 2011 (blue line with circles) and 2003 to 2010 (gray circles). The figure also reports averages over the reference T_{NAT} region (green) introduced in Sect. 3. The potential temperature 450 K corresponded on average to about 18 km altitude throughout the winter (Fig. 7c), and about 55 hPa.

The 2010–2011 Arctic winter stratosphere was close to 2003–2010 values for most targets until mid-January. It then entered the period of remarkably stable cold temperatures discussed in the previous section, and started to significantly differ from the distributions of values observed in previous years. Temperatures in February through March remained at 10 to 20 K below the multi-year average of previous MIPAS-observed years (Fig. 7a). The 2011 N_2O displayed values significantly more constant in time (Fig. 7d), pointing to a slower diabatic descent. The slower descent is also shown by H_2O which was about 20 % below the multi-year average (Fig. 7e), opposite to the weak ascending trend observed in typical years. The cold core of the vortex traced by the T_{NAT} region persisted until early April at a slightly higher altitude. Since in many past Arctic winters the vortex disappeared before spring, it should be noted that the distribution in

ACPD
11, 33191–33227, 2011

time and the multi-year average of 2003–2010 data at a certain date is given by only those years for which the Arctic vortex was defined. In terms of PSCs, the 2010–2011 PSC season extended until mid-March, 2 to 4 weeks longer than recent winters (e.g. Pitts et al., 2011). The altitude range covered by PSCs during 2010–2011 Arctic winter was also anomalous, with PSCs reaching altitudes above 30 km, as compared to maximum altitudes of 29 km previously observed (e.g. Poole and Pitts, 1994; Fromm et al., 1999; Massoli et al., 2006). The observed fraction of 16 % of predominantly NAT PSCs is very close to the 14 % of NAT-only PSCs found by Maturilli et al. (2005) over 1995–2003 using ground based lidar observations.

Nitric acid in the 2011 lower stratosphere was about 40 % lower than the 2003–2010 multi-year average, persisting also when temperatures rose at the end of March (Fig. 7h). This implies denitrification occurred in 2011 as low HNO_3 values persisted even when PSCs disappeared. The most dramatic difference with previous years was however observed in O_3, showing a compact trend that reached values below average only in March (Fig. 7b). With PSCs continuing to form until 18 March at this Θ level, O_3 depletion continued until early April, down to about 50 % of typical values from previous years. NO_2 at $\Theta = 450$ K (Fig. 7f) showed sporadic very high values, likely associated with evaporating PSCs, more often than previous years. In particular, the highest NO_2 values were reached in the last week of February consistently with a period of minimum HNO_3. $ClONO_2$ was close to some previous years until mid-February, then remained significantly depleted (Fig. 7g). The drop in late February to mid-March was coincident with the period of highest ClO (see Fig. 2d) which reached its peak value on 15 March. ClO then started to be converted into its reservoir $ClONO_2$, as shown by the prompt increase of $ClONO_2$ reaching previous years values. This prompt $ClONO_2$ change points to reconversion of ClO into $ClONO_2$ reservoirs rather than (or concomitant to) HCl (compare averages at $\Theta = 550$ K in Fig. 2c and d). The deactivation of ClO stabilized O_3 around 1 ppmv below the range of 2003–2010 values for almost a further month.

ACPD
11, 33191–33227, 2011

These characteristics are similar to the behaviour of the Arctic vortex in the winters 1995-1996 (Manney et al., 1996), 1996–1997 (Newman et al., 1997) and 1999–2000 (Rex et al., 2002; Feng et al., 2005), although this winter the O_3 reduction in the lower stratosphere ($\Theta = 450$–500 K) was deeper and more broadly extended. The O_3 depletion also lasted much longer than during the intense but time-limited depletion observed in 2004-2005 (Manney et al., 2006; Rex et al., 2006), when the PSC season was halted in mid February. The longer 2011 PSC season and the delayed reconversion of ClO into the $ClONO_2$ reservoir caused 2011 daily O_3 depletion rate to reach 100 ppbv day^{-1} (to be compared to the 40 ppbv day^{-1} in 2005, Rex et al., 2006). Given the wider PSC coverage of 2011, this different behaviour is in line with the linear relationship between the total O_3 depletion and the total PSC volume integrated over the winter (as discussed by Harris et al., 2010). Considering the maximum O_3 daily depletion rate reached in mid-March, complete O_3 destruction at $\Theta = 450$ K would have likely occurred in 2011 with only a further week of active chlorine cycles. The observed 2011 denitrification appears to have had a greater role than in previous years, with regions of complete removal of HNO_3 accompanying detection of STS/Mix and NAT PSCs. Although NAT PSCs made of large particles could not be excluded, the much larger fraction of STS/Mix PSC observed suggests their active contribution in driving the lower stratospheric chemistry. If we also consider the O_3 minima reached in the middle stratosphere ($\Theta = 700$–830 K), 2011 showed both the largest NO_x driven ozone depletion above $\Theta = 650$ K as occurred in 2007 (due to the persistent isolation of the upper vortex) and PSC-ClO driven depletion in the lower layers (Kuttippurath et al., 2010).

4.2 Comparison to Antarctic conditions

The above picture is remarkably close to the conditions typically observed over the Antarctic. A comparison to typical conditions of the Antarctic winter is presented in Fig. 8. The figure shows monthly mean vertical profiles of MIPAS2D target quantities in Arctic (blue line with circles for March 2011 and gray lines for the same month in 2003

ACPD
11, 33191–33227, 2011

to 2010), and in the Antarctic (red line with circles for September 2008). March and September have approximately seasonal symmetric conditions in the two hemispheres. Averages were performed on pressure levels and respectively over the 75°-90° N and 75°–90° S geographical latitude, so as to reflect both chemical and dynamical changes of the vortex. Next to temperature and O_3 (Fig. 8, top panels), the figure reports the same targets discussed in the previous section (see labels in the figure). In terms of temperature, altitude, N_2O and H_2O tracers (Fig. 8a, c, d and e), the 2011 Arctic conditions are closer to the Antarctic conditions than to 2003–2010 Arctic winters. The average temperature profile in 2011 resembled the clear vertical *S* shape found in the Antarctic with well defined temperature cold point and stratopause, as opposite to many Arctic winters showing a dynamically-driven almost isothermal lower stratosphere. 2011 N_2O traced a strong isolation of the vortex down to roughly 20 hPa in agreement with the Antarctic N_2O profile. The similarity in the dynamical conditions of the 2011 Arctic and 2008 Antarctic are reflected also in the H_2O profiles. The only Arctic year displaying N_2O and H_2O profiles close to 2011 was 2007 (dashed gray line). Both in the 2011 Arctic and 2008 Antarctic, the altitude of constant pressure surfaces at latitude >75° between 50 and 2 hPa (about 18 and 40 km altitude) was up to 10 % lower than average Arctic conditions.

Beside very similar dynamical conditions, Arctic O_3 reduction in 2011 was less pronounced than in the Antarctic, associated with much weaker denitrification and absence of dehydration below 20 hPa (Fig. 8b, h, and e). At 20 to 10 hPa (which corresponds to the $\Theta = 650$–800 K in the middle stratosphere discussed above) most Arctic parameters are well in agreement with Antarctic conditions, with the exception of a different partitioning of the nitrogen family (see NO_2 and HNO_3 in Fig. 8f and h). In the lower stratosphere, the 2011 Arctic winter ClO was largely deactivated into $ClONO_2$, so that the latter reached higher values in March as compared to Antarctic conditions (Fig. 8g) where ClO generally deactivates through HCl. This implies that although 2011 conditions were closer to the Antarctic than ever before, also 2011 maintained $ClONO_2$ as a channel for ClO deactivation (at the expenses, or together with HCl which we do not

ACPD
11, 33191–33227, 2011

observe). This is in agreement with HCl becoming the dominant reservoir when vortex O_3 drops below 0.5 ppmv as typically reached in the Antarctic (Santee et al., 2008). These values of O_3 were only marginally observed in the 2011 Arctic.

5 Conclusions

We presented MIPAS/ENVISAT observations of 2010–2011 Arctic winter retrieved with a 2-D tomographic approach. The 2010–2011 Arctic winter was characterised by a stronger than usual late vortex with persistent cold temperature, and a PSC season extending until mid-March. In the lower stratosphere, this led to a progressively stronger O_3 depletion correlated with active ClO, until sublimation of PSCs restored the $ClONO_2$ reservoir almost a month later than typical years. In early April, 10 % of vortex O_3 measurements at the 18 km retrieval altitude (about $\Theta = 460$ K) were consistent with total depletion and vortex average O_3 reached 0.6 ppmv. This corresponds to an 80 % chemical loss from the beginning of the winter along the descending 100 ppbv N_2O isopleth. In early January, the detected PSCs reached altitudes above 30 km previously unreported in the Arctic region. About 16 % of the PSCs were classified as NAT, while 84 % PSCs were STS/Mix, pointing to their major role in driving the Arctic chemistry. As compared to 2003–2010 average values, vortex O_3 was lower by 50 % at $\Theta = 450$ K and by 35 % at 550 K in March. In the middle stratosphere ($\Theta = 700$–850 K) O_3 was depleted by 25 % down to 3.3 ppmv, at the lower edge of the 2003–2010 range. 2011 showed the largest ozone depletion ever reported in the Arctic stratosphere.

Our results are largely in agreement with the analysis of the 2010–2011 winter recently published by Manney et al. (2011), which showed ozone hole conditions were reached in the 2011 Arctic. In particular, the lowest vortex average O_3 of 0.6 ppmv which we observed in early April was missed by the Microwave Limb Sounder (MLS) adopted by their study (due to instrumental shut down) but confirmed by two soundings they report for $\Theta = 465$ K (their Fig. 4c). Comparison of our $ClONO_2$ to their HCl trends suggests 2011 Arctic ClO deactivated into $ClONO_2$ rather than HCl which did

ACPD
11, 33191–33227, 2011

not show the same prompt increase. 2011 Arctic conditions were remarkably closer to those observed in the Antarctic than ever before, although they maintained some distinct peculiarities of Arctic winters both in chlorine partitioning and in the composition of PSCs.

The adopted MIPAS2D approach showed a good reproduction of vortex patchy features or filaments of limited (below a few 100 km) dimension through the N_2O tracer, therefore pointing to a similar benefit for active targets. This further motivates the exploitation of the 2-D approach for future studies of scattered low values within the Arctic vortex or ejections of vortex air towards middle latitudes.

Acknowledgements. The authors are grateful to A. Dudhia who first pointed them towards the extreme conditions of the 2010–2011 Arctic winter. The authors are grateful to S. Viscardy and Q. Errera for providing the meteorological data and guidance on how to use them. E. A. and E. P. acknowledge the support by ESA within the framework of the Changing Earth Science Network Initiative.

References

Adriani, A., Massoli, P., Di Donfrancesco, G., Cairo, F., Moriconi, M. L., and Snels, M.: Climatology of polar stratospheric clouds based on lidar observations from 1993 to 2001 over McMurdo Station, Antarctica, J. Geophys. Res.-Atmos., 109, D24211, doi:10.1029/2004JD004800, 2004. 33204

Andrews, D. G., Holton, J. R., and Leovy, C. B.: Middle atmosphere dynamics, Academic Press, New York, NY, USA, 1987. 33193

Carlotti, M., Dinelli, B. M., Raspollini, P., and Ridolfi, M.: Geo-fit Approach to the Analysis of Limb-Scanning Satellite Measurements, Appl. Optics, 40, 1872–1885, doi:10.1364/AO.40.001872, 2001. 33196

Carlotti, M., Brizzi, G., Papandrea, E., Prevedelli, M., Ridolfi, M., Dinelli, B. M., and Magnani, L.: GMTR: Two-dimensional geo-fit multitarget retrieval model for Michelson Interferometer for Passive Atmospheric Sounding/Environmental Satellite observations, Appl. Optics, 45, 716–727, doi:10.1364/AO.45.000716, 2006. 33194, 33196

ACPD

11, 33191–33227, 2011

Carslaw, K. S., Wirth, M., Tsias, A., Luo, B. P., Dörnbrack, A., Leutbecher, M., Volkert, H., Renger, W., Bachmeister, J. T., and Peter, T.: Particle microphysics and chemistry in remotely observed mountain polar stratospheric clouds, J. Geophys. Res., 103, 5785–5796, doi:10.1029/97JD03626, 1998. 33204

Dinelli, B. M., Alpaslan, D., Carlotti, M., Magnani, L., and Ridolfi, M.: Multi-target retrieval (MTR): the simultaneous retrieval of pressure, temperature and volume mixing ratio profiles from limb-scanning atmospheric measurements, J. Quant. Spectrosc. Ra., 84, 141–157, doi:10.1016/S0022-4073(03)00137-7, 2004. 33196

Dinelli, B. M., Arnone, E., Brizzi, G., Carlotti, M., Castelli, E., Magnani, L., Papandrea, E., Prevedelli, M., and Ridolfi, M.: The MIPAS2D database of MIPAS/ENVISAT measurements retrieved with a multi-target 2-dimensional tomographic approach, Atmos. Meas. Tech., 3, 355–374, doi:10.5194/amt-3-355-2010, 2010. 33194, 33196, 33197

Fahey, D. W., Gao, R. S., Carslaw, K. S., Kettleborough, J., Popp, P. J., Northway, M. J., Holecek, J. C., Ciciora, S. C., McLaughlin, R. J., Thompson, T. L., Winkler, R. H., Baumgardner, D. G., Gandrud, B., Wennberg, P. O., Dhaniyala, S., McKinney, K., Peter, T., Salawitch, R. J., Bui, T. P., Elkins, J. W., Webster, C. R., Atlas, E. L., Jost, H., Wilson, J. C., Herman, R. L., Kleinböhl, A., and von König, M.: The Detection of Large HNO_3-Containing Particles in the Winter Arctic Stratosphere, Science, 291, 1026–1031, doi:10.1126/science.1057265, 2001. 33205

Farman, J. C., Gardiner, B. G., and Shanklin, J. D.: Large losses of total ozone in Antarctica reveal seasonal ClO_x/NO_x interaction, Nature, 315, 207–210, doi:10.1038/315207a0, 1985. 33193

Feng, W., Chipperfield, M. P., Davies, S., Sen, B., Toon, G., Blavier, J. F., Webster, C. R., Volk, C. M., Ulanovsky, A., Ravegnani, F., von der Gathen, P., Jost, H., Richard, E. C., and Claude, H.: Three-dimensional model study of the Arctic ozone loss in 2002/2003 and comparison with 1999/2000 and 2003/2004, Atmos. Chem. Phys., 5, 139–152, doi:10.5194/acp-5-139-2005, 2005. 33211

Fischer, H., Birk, M., Blom, C., Carli, B., Carlotti, M., von Clarmann, T., Delbouille, L., Dudhia, A., Ehhalt, D., Endemann, M., Flaud, J. M., Gessner, R., Kleinert, A., Koopman, R., Langen, J., Lpez-Puertas, M., Mosner, P., Nett, H., Oelhaf, H., Perron, G., Remedios, J., Ridolfi, M., Stiller, G., and Zander, R.: MIPAS: an instrument for atmospheric and climate research, Atmos. Chem. Phys., 8, 2151–2188, doi:10.5194/acp-8-2151-2008, 2008. 33194, 33195

Fromm, M. D., Bevilacqua, R. M., Hornstein, J., Shettle, E., Hoppel, K., and Lumpe,

ACPD
11, 33191–33227, 2011

J. D.: An analysis of Polar Ozone and Aerosol Measurement (POAM) II Arctic polar stratospheric cloud observations, 1993–1996, J. Geophys. Res., 1042, 24341–24358, doi:10.1029/1999JD900273, 1999. 33210

Hanson, D. and Mauersberger, K.: Solubility and equilibrium vapor pressures of HC1 dissolved in polar stratospheric cloud materials - Ice and the trihydrate of nitric acid, Geophys. Res. Lett., 15, 1507–1510, doi:10.1029/GL015i013p01507, 1988. 33200

Harris, N. R. P., Lehmann, R., Rex, M., and von der Gathen, P.: A closer look at Arctic ozone loss and polar stratospheric clouds, Atmos. Chem. Phys., 10, 8499–8510, doi:10.5194/acp-10-8499-2010, 2010. 33193, 33211

Höpfner, M., Luo, B. P., Massoli, P., Cairo, F., Spang, R., Snels, M., Di Donfrancesco, G., Stiller, G., von Clarmann, T., Fischer, H., and Biermann, U.: Spectroscopic evidence for NAT, STS, and ice in MIPAS infrared limb emission measurements of polar stratospheric clouds, Atmos. Chem. Phys., 6, 1201–1219, doi:10.5194/acp-6-1201-2006, 2006. 33194, 33198, 33199, 33203

Höpfner, M., Pitts, M. C., and Poole, L. R.: Comparison between CALIPSO and MIPAS observations of polar stratospheric clouds, J. Geophys. Res.-Atmos., 114, D00H05, doi:10.1029/2009JD012114, 2009. 33198, 33199

Kiefer, M., Arnone, E., Dudhia, A., Carlotti, M., Castelli, E., von Clarmann, T., Dinelli, B. M., Kleinert, A., Linden, A., Milz, M., Papandrea, E., and Stiller, G.: Impact of temperature field inhomogeneities on the retrieval of atmospheric species from MIPAS IR limb emission spectra, Atmos. Meas. Tech., 3, 1487–1507, doi:10.5194/amt-3-1487-2010, 2010. 33194

Kuttippurath, J., Godin-Beekmann, S., Lefèvre, F., and Goutail, F.: Spatial, temporal, and vertical variability of polar stratospheric ozone loss in the Arctic winters 2004/2005–2009/2010, Atmos. Chem. Phys., 10, 9915–9930, doi:10.5194/acp-10-9915-2010, 2010. 33194, 33211

Manney, G., Santee, M. L., Rex, M., Livesey, N. J., Pitts, M. C., Veefkind, P., Nash, R. R., Wohltmann, I., Lehmann, R., Froidevaux, L., Poole, L. R., Schoeberl, M. R., Haffner, D. P., Davies, J., Dorokhov, V., Gernandt, H., Johnson, B., Kivi, R., Kyrö, E., Larsen, N., Levelt, P. F., Makshtas, A., McElroy, C. T., Nakajima, H., Parrondo, M. C., Tarasick, D. W., von der Gathen, P., Walker, P. K. A., and Zinoviev, N. S.: Unprecedented Arctic ozone loss in 2011, Nature, 478, 469–475, doi:10.1038/nature10556, 2011. 33194, 33213

Manney, G. L., Zurek, R. W., O'Neill, A., and Swinbank, R.: On the Motion of Air through the Stratospheric Polar Vortex., Journal of Atmospheric Sciences, 51, 2973–2994, doi:10.1175/1520-0469(1994)051¡2973:OTMOAT¿2.0.CO;2, 1994. 33199

ACPD
11, 33191–33227, 2011

Manney, G. L., Santee, M. L., Froidevaux, L., Waters, J. W., and Zurek, R. W.: Polar vortex conditions during the 1995-96 Arctic winter: Meteorology and MLS ozone, Geophys. Res. Lett., 23, 3203–3206, doi:10.1029/96GL02453, 1996. 33194, 33211

Manney, G. L., Santee, M. L., Froidevaux, L., Hoppel, K., Livesey, N. J., and Waters, J. W.: EOS MLS observations of ozone loss in the 2004-2005 Arctic winter, Geophys. Res. Lett., 33, L04802, doi:10.1029/2005GL024494, 2006. 33194, 33199, 33211

Massoli, P., Maturilli, M., and Neuber, R.: Climatology of Arctic polar stratospheric clouds as measured by lidar in Ny-Ålesund, Spitsbergen (79 N, 12 E), J. Geophys. Res.-Atmos., 111, D09206, doi:10.1029/2005JD005840, 2006. 33210

Maturilli, M., Neuber, R., Massoli, P., Cairo, F., Adriani, A., Moriconi, M. L., and Di Donfrancesco, G.: Differences in Arctic and Antarctic PSC occurrence as observed by lidar in Ny-Ålesund (79° N, 12° E) and McMurdo (78° S, 167° E), Atmos. Chem. Phys., 5, 2081–2090, doi:10.5194/acp-5-2081-2005, 2005. 33210

Molina, M. J., Tso, T., Molina, L. T., and Wang, F.: Antarctic Stratospheric Chemistry of Chlorine Nitrate, Hydrogen Chloride, and Ice: Release of Active Chlorine, Science, 238, 1253–1257, doi:10.1126/science.238.4831.1253, 1987. 33193

Newman, P. A., Gleason, J. F., McPeters, R. D., and Stolarski, R. S.: Anomalously low ozone over the Arctic, Geophys. Res. Lett., 24, 2689–2692, doi:10.1029/97GL52831, 1997. 33211

Papandrea, E., Arnone, E., Brizzi, G., Carlotti, M., Castelli, E., Dinelli, B. M., and Ridolfi, M.: Two-dimensional tomographic retrieval of MIPAS/ENVISAT measurements of ozone and related species, Int. J. Remote Sens., 31, 477–483, doi:10.1080/01431160902893501, 2010. 33196

Pitts, M. C., Poole, L. R., Dörnbrack, A., and Thomason, L. W.: The 2009–2010 Arctic polar stratospheric cloud season: a CALIPSO perspective, Atmos. Chem. Phys., 11, 2161–2177, doi:10.5194/acp-11-2161-2011, 2011. 33210

Poole, L. R. and Pitts, M. C.: Polar stratospheric cloud climatology based on Stratospheric Aerosol Measurement II observations from 1978 to 1989, J. Geophys. Res., 991, 13083–13090, doi:10.1029/94JD00411, 1994. 33210

Proffitt, M. H., Margitan, J. J., Kelly, K. K., Loewenstein, M., Podolske, J. R., and Chan, K. R.: Ozone loss in the Arctic polar vortex inferred from high-altitude aircraft measurements, Nature, 347, 31–36, doi:10.1038/347031a0, 1990. 33207

Randel, W. J. and Wu, F.: Cooling of the Arctic and Antarctic Polar Stratospheres due to Ozone Depletion, J. Climate, 12, 1467–1479, doi:10.1175/1520-

ACPD
11, 33191–33227, 2011

0442(1999)012¡1467:COTAAA¿2.0.CO;2, 1999. 33193
Remedios, J. and Spang, R.: Detection of cloud effects in MIPAS spectral data and implications for the MIPAS operational processor, in: ENVISAT calibration review, edited by: Sawaya-Lacoste, H., ESA SP-520, Noordwijk, The Netherlands, 2002. 33198
Rex, M., Salawitch, R. J., Harris, N. R. P., von der Gathen, P., Braathen, G. O., Schulz, A., Deckelmann, H., Chipperfield, M., Sinnhuber, B.-M., Reimer, E., Alfier, R., and *et al.*: Chemical depletion of Arctic ozone in winter 1999/2000, J. Geophys. Res.-Atmos., 107, 8276, doi:10.1029/2001JD000533, 2002. 33194, 33207, 33211
Rex, M., Salawitch, R. J., Deckelmann, H., von der Gathen, P., Harris, N. R. P., Chipperfield, M. P., Naujokat, B., Reimer, E., Allaart, M., Andersen, S. B., Bevilacqua, R., Braathen, G. O., Claude, H., Davies, J., De Backer, H., Dier, H., Dorokhov, V., Fast, H., Gerding, M., Godin-Beekmann, S., Hoppel, K., Johnson, B., Kyrö, E., Litynska, Z., Moore, D., Nakane, H., Parrondo, M. C., Risley, A. D., Skrivankova, P., Stübi, R., Viatte, P., Yushkov, V., and Zerefos, C.: Arctic winter 2005: Implications for stratospheric ozone loss and climate change, Geophys. Res. Lett., 33, L23808, doi:10.1029/2006GL026731, 2006. 33193, 33211
Santee, M. L., MacKenzie, I. A., Manney, G. L., Chipperfield, M. P., Bernath, P. F., Walker, K. A., Boone, C. D., Froidevaux, L., Livesey, N. J., and Waters, J. W.: A study of stratospheric chlorine partitioning based on new satellite measurements and modeling, J. Geophys. Res.-Atmos., 113, D12307, doi:10.1029/2007JD009057, 2008. 33213
Solomon, S.: Stratospheric ozone depletion: A review of concepts and history, Rev. Geophys., 37, 275–316, doi:10.1029/1999RG900008, 1999. 33193
Solomon, S., Garcia, R. R., Rowland, F. S., and Wuebbles, D. J.: On the depletion of Antarctic ozone, Nature, 321, 755–758, doi:10.1038/321755a0, 1986. 33193
Spang, R., Remedios, J. J., Kramer, L. J., Poole, L. R., Fromm, M. D., Müller, M., Baumgarten, G., and Konopka, P.: Polar stratospheric cloud observations by MIPAS on ENVISAT: detection method, validation and analysis of the northern hemisphere winter 2002/2003, Atmos. Chem. Phys., 5, 679–692, doi:10.5194/acp-5-679-2005, 2005. 33198
Stein, B., Wedekind, C., Wille, H., Immler, F., Müller, M., Wöste, L., del Guasta, M., Morandi, M., Stefanutti, L., Antonelli, A., Agostini, P., Rizi, V., Readelli, G., Mitev, V., Matthey, R., Kivi, R., and Kyrö, E.: Optical classification, existence temperatures, and coexistence of different polar stratospheric cloud types, J. Geophys. Res., 1042, 23983–23994, doi:10.1029/1999JD900064, 1999. 33203
Tomasi, C., Petkov, B., Maria Dinelli, B., Castelli, E., Arnone, E., and Papandrea,

ACPD
11, 33191–33227, 2011

E.: Monthly mean vertical profiles of pressure, temperature and water vapour volume mixing ratio in the polar stratosphere and low mesosphere from a multi-year set of MIPAS-ENVISAT limb-scanning measurements, J. Atmos. Sol.-Terr. Phys., 73, 2237–2271, doi:10.1016/j.jastp.2011.06.018, 2011. 33197

WMO: Scientific Assessment of Ozone Depletion: 2006, Global Ozone Monitoring and Research Project-Report, Project-Report 50, World Meteorological Organisation, Geneva, Switzerland, 572 pp., 2007. 33193, 33194

ACPD

11, 33191–33227, 2011

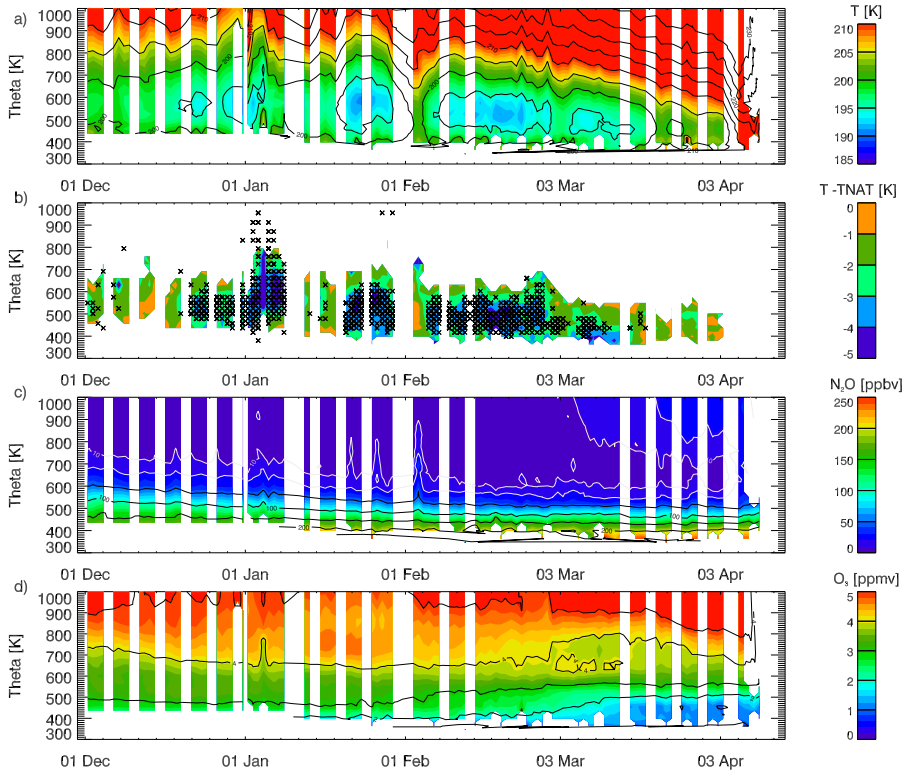

Fig. 1. Timeseries of MIPAS2D vortex average temperature, T_{NAT} region average temperature, vortex average N_2O and O_3 (top to bottom). The T_{NAT} region temperature in panel **(b)** is shown in terms of the difference $T - T_{NAT}$. Panel **(b)** also shows the altitude of PSCs detected through MIPAS spectra (black crosses). White vertical regions depict periods without MIPAS2D data.

ACPD
11, 33191–33227, 2011

MIPAS2D view of ozone depletion in 2010–2011 Arctic winter

E. Arnone et al.

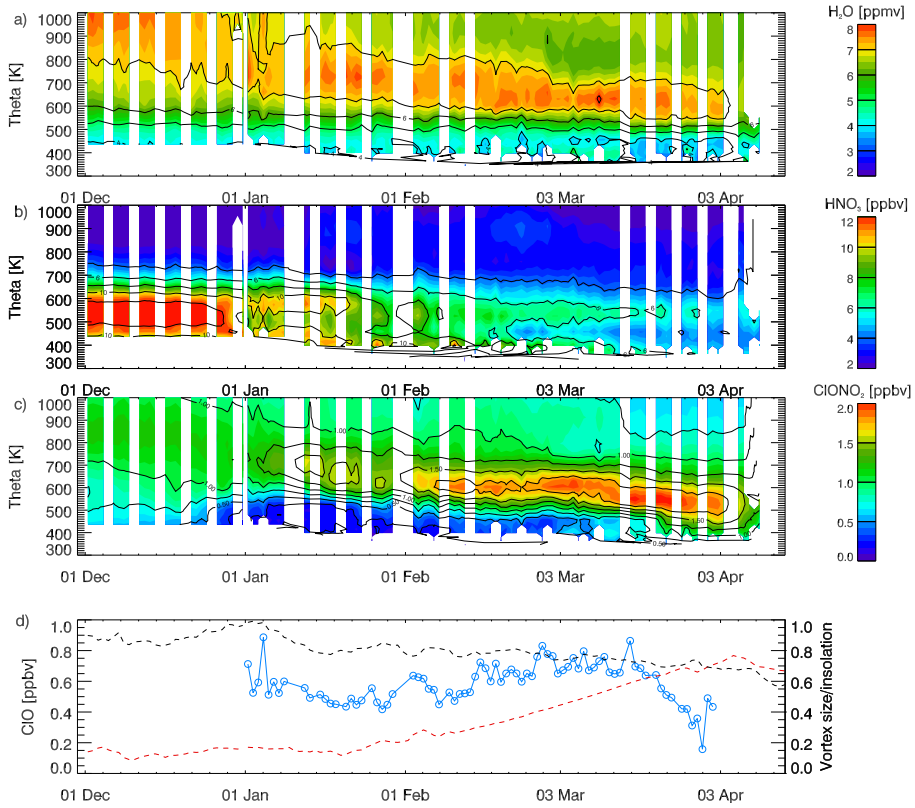

Fig. 2. Timeseries of MIPAS2D vortex-averaged H_2O, HNO_3, $ClONO_2$ and ClO (top to bottom). ClO in **(d)** is shown only as vortex average of am measurements at $\Theta = 550$ K (blue). **(d)** reports also the evolution of the vortex area (black dashed line) in terms of fraction to its maximum extent (25×10^6 km^2) and the vortex sunlit daily fraction (red dashed line) both calculated at $\Theta = 550$ K (refer to right vertical axis). White vertical regions depict periods without MIPAS2D data.

ACPD
11, 33191–33227, 2011

MIPAS2D view of ozone depletion in 2010–2011 Arctic winter

E. Arnone et al.

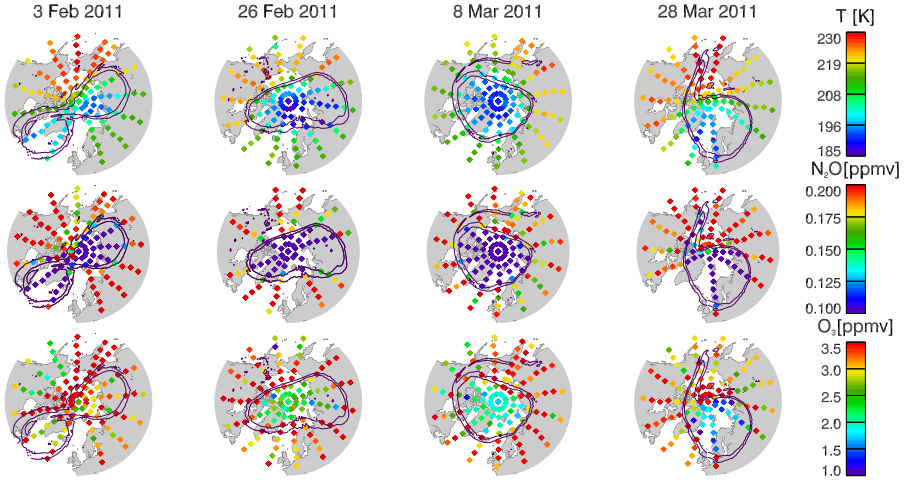

Fig. 3. Snapshots of MIPAS2D temperature, N_2O and O_3 (top to bottom) along MIPAS orbits on the 500 K isentrope during selected days in February and March 2011. Only MIPAS am measurements are shown. Black contour lines of constant sPV trace the outer and inner edge of the vortex (respectively with sPV = 1.4×10^{-4} s^{-1} and 2×10^{-4} s^{-1}).

ACPD
11, 33191–33227, 2011

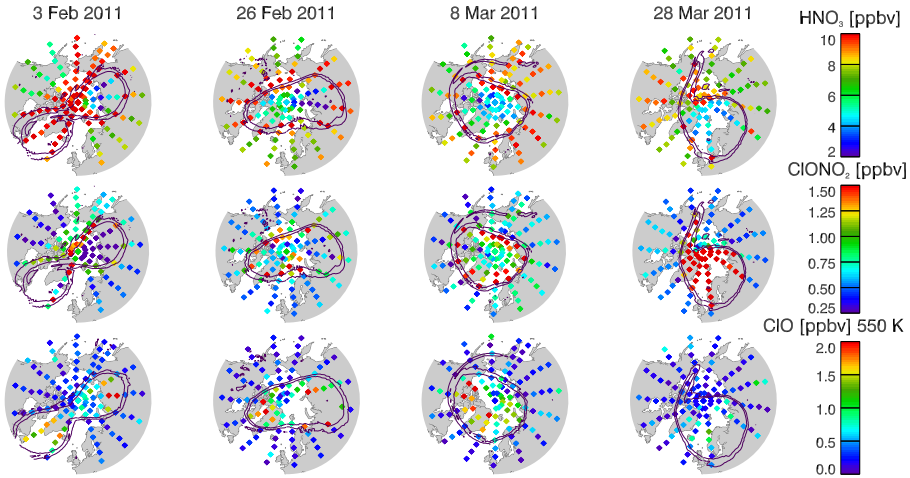

Fig. 4. As in Fig. 3 but for HNO_3, $ClONO_2$, and ClO (top to bottom). ClO is shown on the 550 K isentrope (see text for details).

ACPD
11, 33191–33227, 2011

MIPAS2D view of ozone depletion in 2010–2011 Arctic winter

E. Arnone et al.

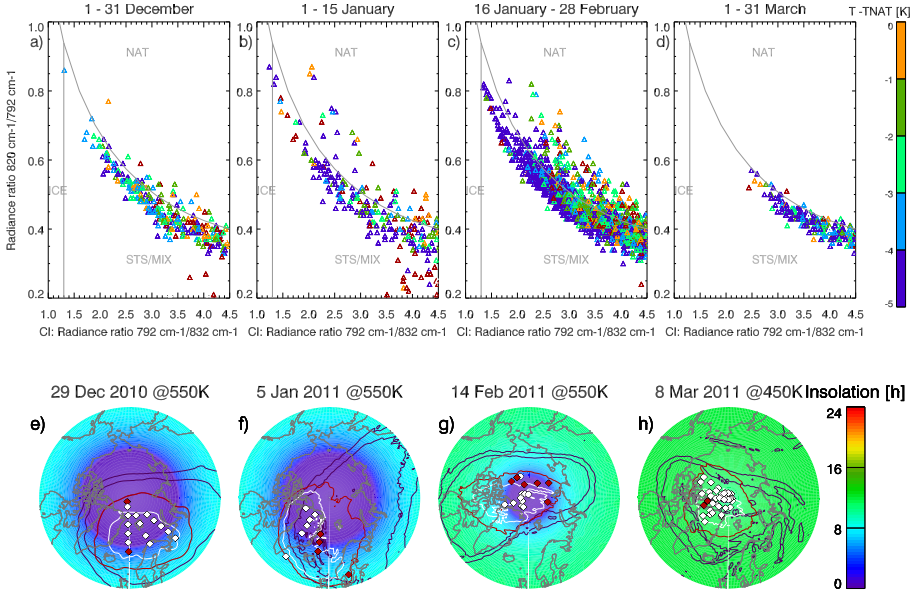

Fig. 5. Classification of MIPAS detected PSCs in the four periods: 1–31 December 2010, 1–15 January 2011, 16 January–28 February, and 1–31 March 2011 (left to right top panels) derived from spectral ratios at the cloud top. Colors indicate the difference between the ECMWF temperature coincident with the detected PSC and the estimated T_{NAT} threshold (red is above T_{NAT}). Bottom panels report the PSCs classified as NAT (red diamonds) and STS/Mix (white diamonds) over maps of the average number of daily sunlit hours during selected days of the four periods. Also shown are regions of predicted PSC occurrence based on ECMWF temperature (red line: NAT region where $T - T_{NAT} < 0$; white line: STS region where $T - T_{NAT} < -3.5$ K). Vortex edges (black lines) are shown as in Fig. 3.

ACPD
11, 33191–33227, 2011

MIPAS2D view of ozone depletion in 2010–2011 Arctic winter

E. Arnone et al.

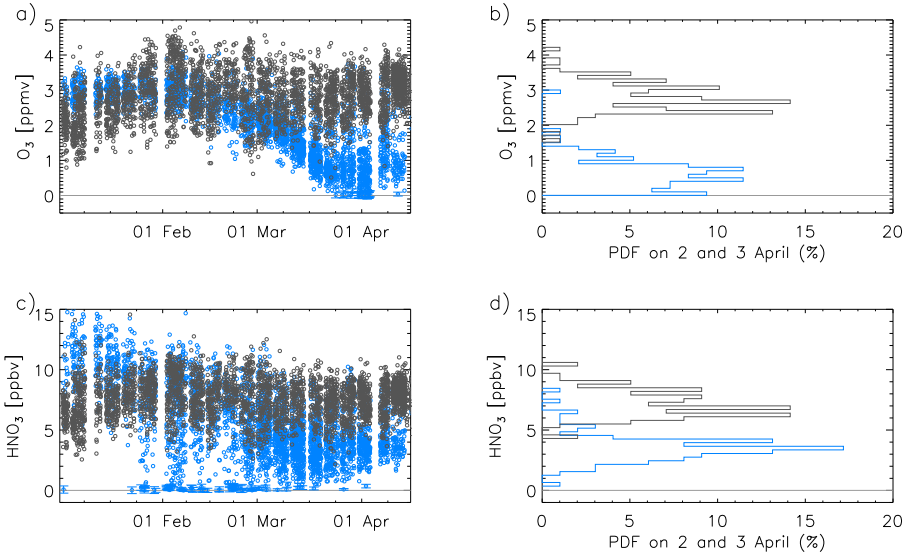

Fig. 6. Timeseries (left) and probability distribution functions (PDFs) on 2–3 April 2011 (right) of MIPAS2D individual measurements of O_3 (top) and HNO_3 (bottom) at the 18 km retrieval grid point and North of 65° geographical latitude. Vortex (blue) and outside vortex (gray) data are shown. In the timeseries panels (left), error bars are shown only for measurements close to zero.

ACPD
11, 33191–33227, 2011

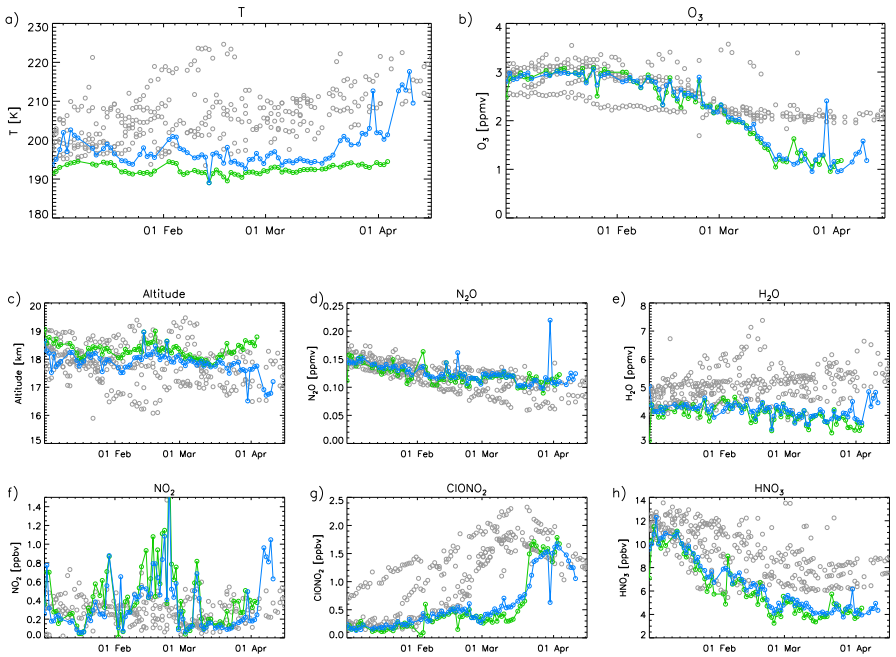

Fig. 7. Timeseries of daily vortex-averaged MIPAS2D targets on the 450 K isentrope during January to April for individual years 2003 to 2010 (gray circles) and 2011 (blue). MIPAS2D 2011 data averaged within the T_{NAT} region (green) are also shown. Targets are temperature and O_3 (top panels), altitude of retrieved data, N_2O and H_2O (middle panels), NO_2, $ClONO_2$ and HNO_3 (bottom panels).

ACPD
11, 33191–33227, 2011

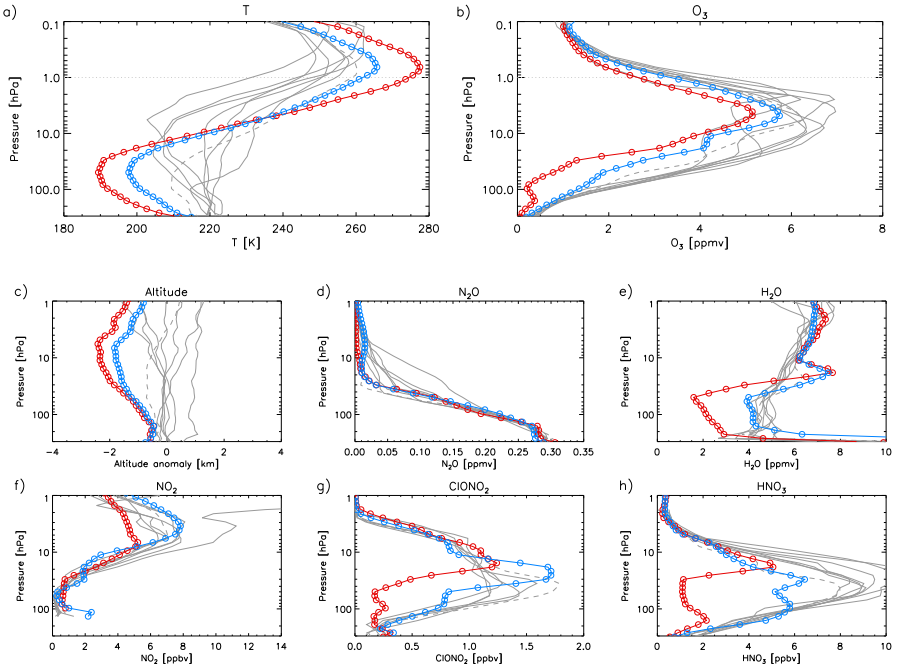

Fig. 8. MIPAS2D monthly mean vertical profiles for selected targets in Arctic for March 2011 (blue line with circles) and 2003 to 2010 (gray lines; 2007 dashed), and in Antarctic for September 2008 (red line with circles). Data are averaged poleward of 75° geographical latitude. Targets are temperature and O_3 (top panels), altitude of retrieved data, N_2O and H_2O (middle panels), NO_2, $ClONO_2$ and HNO_3 (bottom panels). The altitude is shown as difference to the 2003–2010 Arctic average. Note that profiles extend from 300 to 1 hPa, apart from temperature and O_3 extending up to 0.1 hPa.

ACPD
11, 33191–33227, 2011